Multi-objective aerodynamic optimization design of high-speed maglev train nose

Shuanbao Yao, Dawei Chen and Sansan Ding
National Engineering Research Center for High-speed EMU Engineer, CRRC Qingdao Sifang Limited Company, Qingdao, China

Received 19 February 2022
Revised 5 March 2022
Accepted 18 April 2022

Abstract

Purpose – The nose length is the key design parameter affecting the aerodynamic performance of high-speed maglev train, and the horizontal profile has a significant impact on the aerodynamic lift of the leading and trailing cars Hence, the study analyzes aerodynamic parameters with multi-objective optimization design.

Design/methodology/approach – The nose of normal temperature and normal conduction high-speed maglev train is divided into streamlined part and equipment cabin according to its geometric characteristics. Then the modified vehicle modeling function (VMF) parameterization method and surface discretization method are adopted for the parametric design of the nose. For the 12 key design parameters extracted, combined with computational fluid dynamics (CFD), support vector machine (SVR) model and multi-objective particle swarm optimization (MPSO) algorithm, the multi-objective aerodynamic optimization design of high-speed maglev train nose and the sensitivity analysis of design parameters are carried out with aerodynamic drag coefficient of the whole vehicle and the aerodynamic lift coefficient of the trailing car as the optimization objectives and the aerodynamic lift coefficient of the leading car as the constraint. The engineering improvement and wind tunnel test verification of the optimized shape are done.

Findings – Results show that the parametric design method can use less design parameters to describe the nose shape of high-speed maglev train. The prediction accuracy of the SVR model with the reduced amount of calculation and improved optimization efficiency meets the design requirements.

Originality/value – Compared with the original shape, the aerodynamic drag coefficient of the whole vehicle is reduced by 19.2%, and the aerodynamic lift coefficients of the leading and trailing cars are reduced by 24.8 and 51.3%, respectively, after adopting the optimized shape modified according to engineering design requirements.

Keywords Design of head shape, Maglev train, Aerodynamic parameter, Multi-objective optimization, Parametric design

Paper type Research paper

1. Introduction

The design speed of normal temperature and normal conduction high-speed maglev trains in China ("high-speed maglev trains") has reached 600 km · h^{-1}, and the aerodynamic effect has a greater influence on the stability and riding comfort of the trains at a high speed (Yang, Guo, Yao, & Liu, 2012; Britcher, Wells, & Renaud, 2012; Tielkes, 2006). As a result, the aerodynamic design has become an important and difficult issue in the shape design of high-speed maglev trains. High-speed maglev trains float above the track with no contact, and the maglev propulsion supports the trains' loading and running. The mechanical friction resistance is negligible, and the aerodynamic drag is the main resistance source to be overcome by running high-speed maglev trains (Shu, Gu, & Liang, 2006; Ma, Zhou, & Zhao, 2013). The design of the

Railway Sciences
Vol. 1 No. 2, 2022
pp. 273-288
Emerald Publishing Limited
e-ISSN: 2755-0915
p-ISSN: 2755-0907
DOI 10.1108/RS-04-2022-0017

maglev control system needs to consider the fluctuation amplitude and average value of the aerodynamic lift of each car (Yau, 2010; Ding, Yao, & Chen, 2020; Li, Liu, & Zhai, 2004). Therefore, the nose design is one of the important means used to improve the aerodynamic performance of high-speed maglev trains (Liu, Tian, & Wang, 2006; Bi, Lei, & Zhang, 2004).

The high-speed maglev train and the high-speed train have similar shapes, both of them are near-ground running objects with a high slenderness ratio (Yao, Guo, & Yang, 2012; Yao, Guo, Sun, Yang, & Chen, 2014). However, compared with the high-speed train, the high-speed maglev train hovers above the track, it has no complex exposed components, such as bogie and pantograph, and its equipment cabin is connected to the track beam in a circular manner (Ding *et al.*, 2020). The parametric nose design methods of the high-speed train are inapplicable to the high-speed maglev train (Yao, Guo, Sun, Chen, & Yang, 2014; Ku, Park, & Kwak, 2010; Gong, Sun, & Li, 2019; Rho, Ku, & Kee, 2009). Besides, in order to ensure an effective maglev guiding system, the gap between the floor of the normal-conducting high-speed maglev train and the track beam is very small, and the minimum gap is measured in millimeter. When the underfloor equipment cabin is fully sealed, an upward aerodynamic lift force acts on both the leading car and the trailing car (Ding *et al.*, 2020). However, the aerodynamic force on the leading car of the high-speed train is a downward pressure and that on the trailing car is an upward force, which is smaller (Yang *et al.*, 2012). Therefore, the nose aerodynamic optimization design methods and objectives have difference between the high-speed maglev train and the high-speed train. In order to improve the efficiency of the aerodynamic performance of trains, it is necessary to carry out studies on the aerodynamic optimization design of nose according to the structural characteristics of the high-speed maglev train.

This paper carries out parametric design of the streamlined part and the equipment cabin of the nose of high-speed maglev train by using the modular support vector machine (SVR) parametric method (Yao *et al.*, 2016; Rho *et al.*, 2009); it carries out the study on aerodynamic optimization design of the nose of the high-speed maglev train and analyze the sensitivity of key design parameters to the optimization objectives by using the SVR model and the multi-objective particle swarm optimization (MPSO) algorithm so as to optimize the aerodynamic drag coefficient of the train and the aerodynamic lift coefficient of the leading and trailing cars.

2. Numeral calculation methodology

2.1 Calculation model

In the calculation model of high-speed maglev train, the real dimensions of straight tracks and the real shape of three-car high-speed maglev train are adopted, the impact of antennas on the aerodynamic performance of maglev train is not taken into consideration and the windshield is simplified to a full windshield, as shown in Figure 1. The streamlined parts of leading and trailing cars are studied for the nose optimization design of the high-speed maglev train. In the nose optimization design, the geometric shape of other components of the train and the total length of the train remains unchanged.

The design speed of the high-speed maglev train is 600 km/h. The impact of the air compression effect on the aerodynamic performance of the train at this speed is very

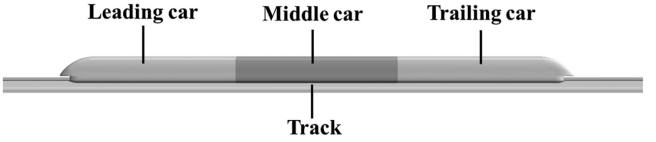

Figure 1.
Calculation model of high-speed maglev train

significant. Therefore, the numerical calculation method and the boundary layer area grid processing method suggested by Ding *et al.* (2020) are adopted.

Calculation area: The length of the train L is adopted as the characteristic length, the distance from the inflow boundary to the nose tip of the leading car is equal to L, the distance from the outlet boundary to the nose tip of the trailing car is equal to $2L$, the outfield height is L and the distance from the outfield side boundary to the centerline of the train is equal to L, as shown in Figure 2.

Boundary conditions: The inflow speed is 600 $km \cdot h^{-1}$, the far-field pressure is one atmospheric pressure (101.325 kPa) and the temperature T is 288 K. As the calculation model is compressible, the far-field boundary is set to the nonreflecting boundary, and the ground, track and carbody are set to the no-slip wall. To simulate the relative movement between the high-speed maglev train and the ground facilities, the ground and the track are set to the moving wall with the moving speed equal to the inflow speed.

2.2 Verification of grid independence

In order to verify the impact of the grid division on the result of the aerodynamic load calculation, tri-prism grids are divided on the fixed wall boundary, and spatial grids are divided into orthogonal hexahedral grids. On the premise that the thickness of the grids of the first boundary layer meets the requirement of the wall function, a total of four sets of grids are divided. The quantities of their grids are 33.82 m, 44.99 m, 54.37 m and 98.96 m, respectively. The set of 33.82 m grids corresponds to the carbody surface and the distribution of grids in the calculation area as shown in Figure 3.

For analysis purposes, unless otherwise specified, the aerodynamic loads on the high-speed maglev train are expressed in the dimensionless form.

The aerodynamic drag coefficient C_d is as follows:

$$C_d = \frac{F_d}{0.5\rho v^2 S} \tag{1}$$

The aerodynamic lift coefficient C_l is as follows:

$$C_l = \frac{F_l}{0.5\rho v^2 S} \tag{2}$$

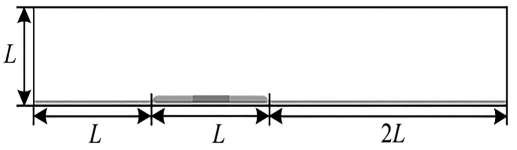

Dimensions of far-field parallel to inflow direction

(a)

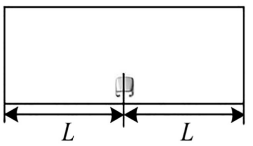

Dimensions of far-field perpendicular to inflow direction

(b)

Figure 2.
Dimensions of calculation area

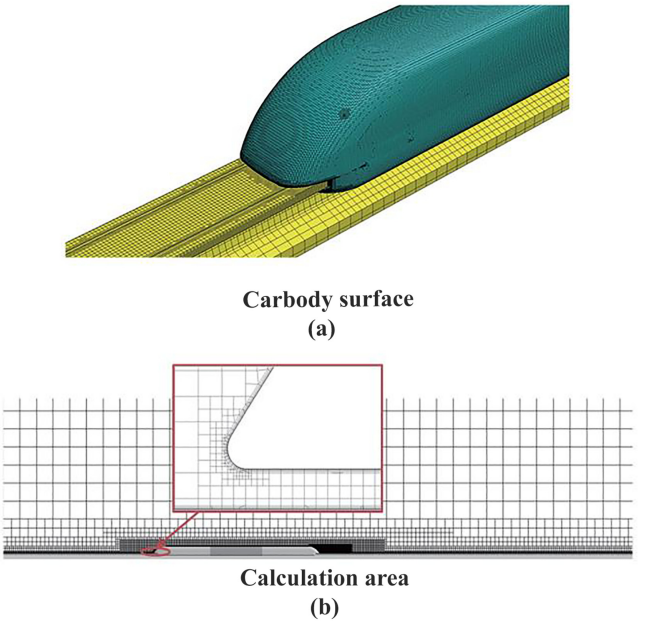

Figure 3.
Carbody surface and distribution of grids in calculation area (33.82 million grids)

where F_d is the aerodynamic drag; F_1 is the aerodynamic lift; ρ is the air density, equal to 1.225 $kg \cdot m^{-3}$; v is the running speed of high-speed maglev train or the inflow speed during wind tunnel test; S is the maximum cross-section area of carbody, i.e. 11.87 m^2.

The calculation results of the aerodynamic coefficients when different grid division methods are used are shown in Figure 4.

According to Figure 4, the calculation results in the case of different quantities of grids are not so different. The difference between the aerodynamic drag coefficients of the train and the between the aerodynamic lift coefficients of the leading car and the middle car is less than 5%, and the difference between the aerodynamic lift coefficients of the trailing car is less than 7%. Therefore, the grid division mode only has a small impact on the calculation results. In order to improve the efficiency of flow field calculation, the division of 33.82 million grids is adopted below.

3. Aerodynamic optimization design of nose

3.1 Optimization process

In order to improve the efficiency of the nose optimization design of the high-speed maglev train, the SVR model is introduced, and 50 sample points are collected with the Latin hypercube sampling method (Shao, Zhang, & Yang, 2013). In the 50 sample points, 46 are randomly selected and used as training sample points, and the remaining four points are used as test sample points. Each optimization objective corresponds to one set of SVR model. In the design space, the aerodynamic drag coefficient of the train varies within a narrow range and the aerodynamic lift coefficient of leading and trailing cars a wide range. Therefore, in order to reduce the number of samples and improve the optimization efficiency, when the average prediction error of the SVR model based on the aerodynamic drag coefficient of the train is lower than 5% and the maximum prediction error is lower than 10%, they satisfy the design requirements; when the average prediction error of the SVR model based on the aerodynamic

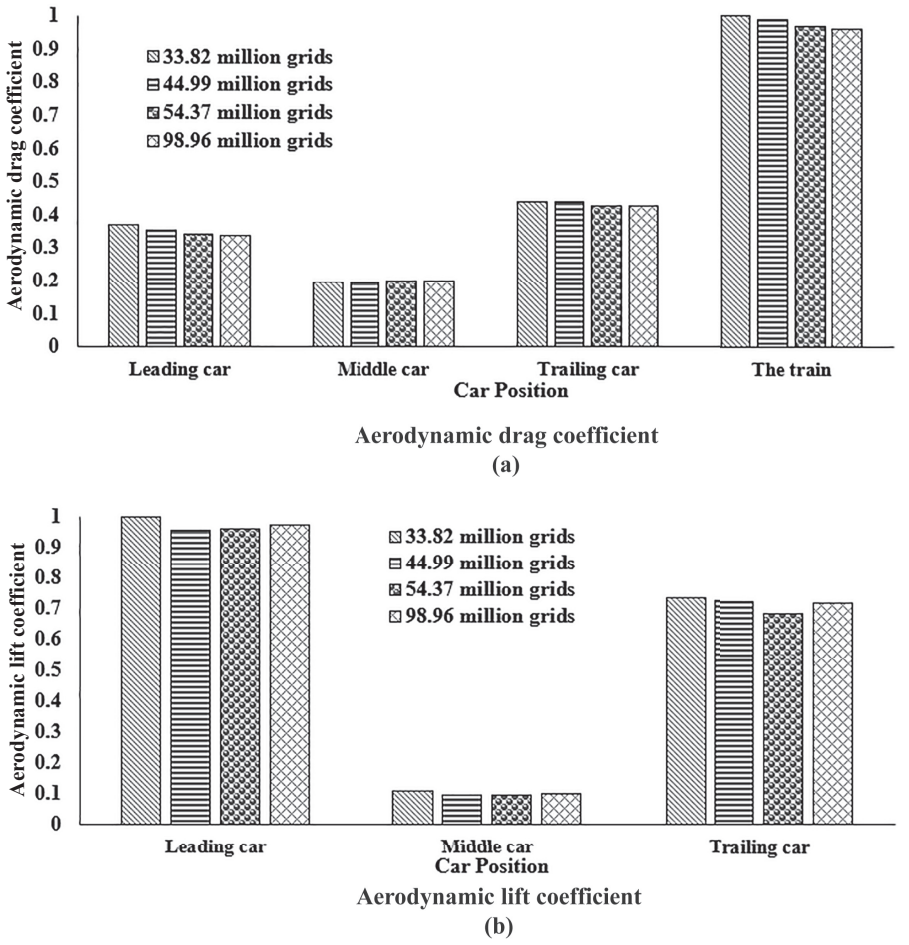

Figure 4.
Aerodynamic coefficients of train in case of different quantities of grids

lift coefficient of leading and trailing cars is lower than 10% and the maximum prediction error is lower than 15%, they satisfy the design requirements.

The process of nose optimization design of high-speed maglev train based on the SVR model is shown in Figure 5. The steps are described below.

Step 1: Carry out parametric design according to the original shape and geometric constraints, set the design space (value range of design parameters), determine the number of sample points based on the generalization capability of the SVR model, obtain sample points by using the sampling method and work out the optimization objective values corresponding to each sample point by using the computational fluid dynamics (CFD) method to form a set of initial training sample points;

Step 2: Build the corresponding SVR model for each optimization objective by using the set of initial training sample points and the single-objective particle swarm algorithm (PSO). Namely, build three sets of SVR models for the aerodynamic drag of a three-car train (SVR-C_{rd}), for the aerodynamic lift of the leading car (SVR-C_{Hl}) and for the aerodynamic lift of the trailing car (SVR-C_{Tl});

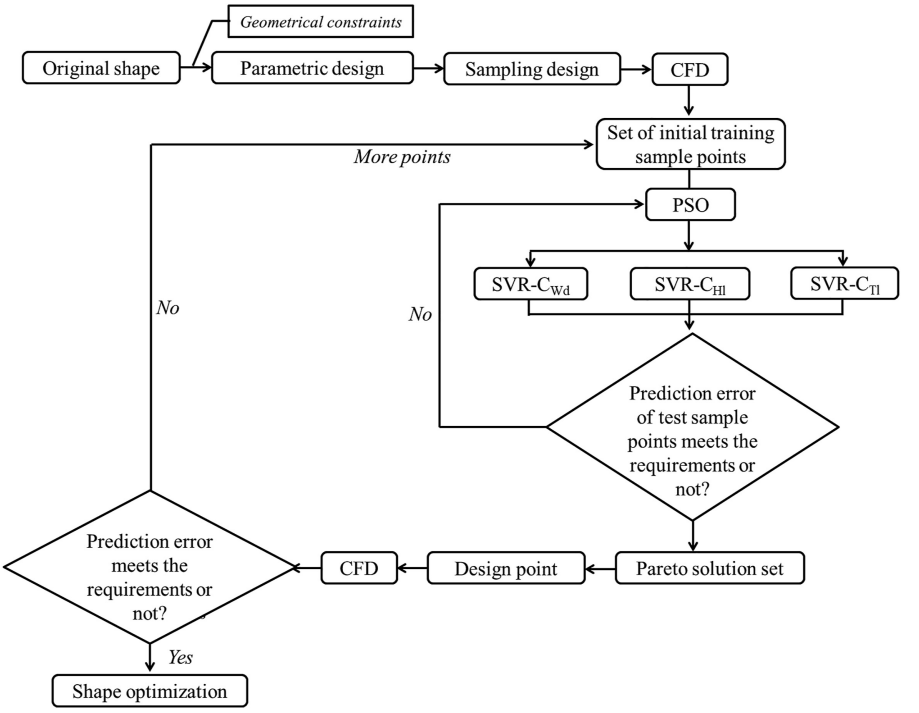

Figure 5.
Process of nose optimization of high-speed maglev train

Step 3: Integrate the response surface models of the SVRs to form a set of the final response surface models of SVRs and use it as the response surface model called by the MPSO algorithm;

Step 4: Work out aerodynamic coefficients by using the established SVR model and carry out optimization in the design space by using the MPSO algorithm to obtain the Pareto solution set;

Step 5: Randomly select some design points from the Pareto optimal solution set for CFD verification and judge whether the prediction accuracy of the SVR model meets the requirements based on this. If the prediction accuracy meets the requirements, select the final optimized shape according to the preference of the optimization objective and the optimization process ends at this time; if the prediction accuracy fails to meet the requirements, go back to Step 2 and retrain the SVR model.

3.2 Parametric design

The nose of the high-speed maglev train based on the normal conducting maglev technology is streamlined, and the cross-section of the carbody is in a channel shape. The geometric shape is composed of several complex curved surfaces. In the design, the curved surfaces are subject to very large deformation and their types vary. In view of the characteristics of the high-speed maglev train nose, based on the idea of parametric design for different parts, the nose is divided into two parts: the streamlined part and the equipment cabin. The parametric design of the streamlined part is carried out by using the improved vehicle modeling function

(VMF) parametric method, and the parametric design of the equipment cabin is carried out by using the curved surface discrete method (Yao *et al.*, 2016).

The critical control lines of the nose geometry of the high-speed maglev train are shown in Figure 6 where x is the coordinate along the length of the nose; y is the coordinate along the width of the nose; z is the coordinate along the height of the nose; L1–L4 and R1–R7 are control lines; K1–K5 are the endpoints of the control lines and S1 is the separation point of the straight segment and the curve segment of L2.

The improved VMF parametric method controls the shape of curved surfaces of the nose by controlling the lines. The nose of the high-speed maglev train is symmetric along the longitudinal section. To facilitate the development of the parametric program, the parametric design of the nose is conducted only on the curved surfaces on the one side and those on the other side are symmetric. According to Figure 6, the shape of the longitudinal section is controlled by L1, that of the horizontal section L2 and that of the front end of the equipment cabin L3; the shape of the maximum cross-section is controlled by L4; since the curves of L4 are the most complex, it is divided into seven different types of curves, i.e. R1–R7; R1 is used for the parametric design of the streamlined part and R2–R7 for the parametric design of the equipment cabin. The shape of the maximum cross-section of the carbody depends on factors such as vehicle clearance limit, equipment layout and the matching relationship between existing cars. Therefore, the parametric design of L4 is not carried out, and it used as the boundary line of the nose-curved surfaces.

Since the high-speed maglev train is an automated vehicle, the view angle of the driver's cab and the impact of glass on the driver's view are not considered. Therefore, the shape of the streamlined part is changed by controlling L1, L2 and the air guiding channel at the nose tip.

In order to facilitate the analysis of parametric expressions, the coordinates system of each control line may be determined according to the coordinates of the endpoint of the line by using the unified coordinates system as shown in Figure 6.

L1 is the longitudinal section line of the nose, and the y-coordinate is 0. In order to ensure the consistency of the shape control expression of L1, the length of L1 is unitized into 1, and the shape control expression of L1 is as follows:

$$z(x) = \left(\frac{x - x_1}{x_2 - x_1}\right)^{w_2} \left(1 - \frac{x - x_1}{x_2 - x_1}\right)^{2.5} w_3 \left(1 - \frac{x - x_1}{x_2 - x_1}\right)^{w_4} + 2(z_2 - z_1)\frac{x - x_1}{x_2 - x_1} - (z_2 - z_1)\frac{x - x_1}{x_2 - x_1} - (z_2 - z_1)\left(\frac{x - x_1}{x_2 - x_1}\right)^2 \tag{3}$$

where, (x_1, z_1) are the coordinates of the starting point of L1, located at the nose tip, i.e. point K1; (x_2, z_2) are the coordinates of the endpoint of L1, located at the center on the top of the maximum cross-section of the carbody; w_2, w_3 and w_4 are the design parameters of L1.

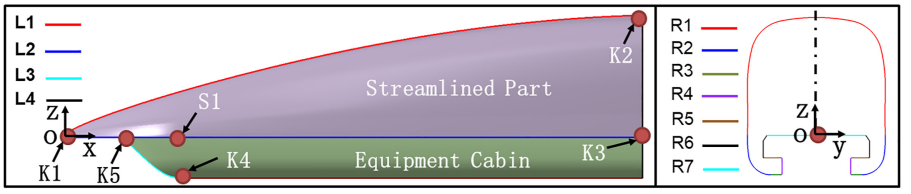

Figure 6.
Critical control lines of nose geometry of high-speed maglev train

The z-coordinate of control line L1 obtained from formula (3) can be converted into the real coordinate z' by multiplying it by the nose length w_1:

$$z'(x) = w_1 z(x) \tag{4}$$

L2 is the bottom boundary of the streamlined part and the top boundary of the equipment cabin, and its z-coordinate remains unchanged. Limited by the space accommodating the levitation frame, from the maximum cross-section of the carbody to separation point S1 as shown in Figure 6, the equipment cabin should be a straight-pattern tensile surface, and L2 in this section should be straight. However, the shape of the curve section from S1 to the nose tip is variable. Therefore, the parametric design focuses on L2 in this section, and the shape control expression is as follows:

$$\begin{aligned} y(x) = &\left(\frac{x - x_1}{x_3 - x_1}\right)^{w_5}\left(1 - \frac{x - x_1}{x_3 - x_1}\right)w_6\left(1 - \frac{x - x_1}{x_3 - x_1}\right)^{w_6} + \\ &2(y_3 - y_1)\frac{x - x_1}{x_3 - x_1} - (y_3 - y_1)\left(\frac{x - x_1}{x_3 - x_1}\right)^2 \end{aligned} \tag{5}$$

where (x_1, y_1) are the coordinates of the starting point of L2, and like L1, the starting point of L2 is also located at the nose tip; (x_3, y_3) are the coordinates of the endpoint of L2, i.e. point S1; w_5, w_6 and w_7 are the design parameters of L2.

The shape of the curved surface at the front end of the equipment cabin has a great influence on the aerodynamic performance of the high-speed maglev train, which is most sensitive to the inclination angle of the curved surface projection on the zx plane. Therefore, L3 is considered an oblique line projected on the zx plane, with the y-coordinate unchanged. The shape control expression is as follows:

$$x(z) = x_5 + \frac{z - z_4}{z_5 - z_4}(x_4 - x_5) \tag{6}$$

where (x_4, z_4) are the coordinates of the lower endpoint of L3; x_4 is taken as the design parameter w_9; (x_5, z_5) are the coordinates of the upper endpoint of L3 and x_5 is taken as the design parameter w_8.

The spatial curved surface of the high-speed maglev train nose is obtained by interpolation according to formulas (7) and (8). For spatial curved surface interpolation, the spatial curve interpolation may be performed along the x-direction to discretize the entire curved surface into regular spatial grid points whose coordinates are used to represent the curved surface data. Therefore, when the spatial curved surface of the high-speed maglev train nose is obtained by interpolation, the spatial points in the y-direction are set to be evenly distributed. Namely, the x-coordinate of the curved surface control line remains unchanged, the distance in the y-direction is divided into nt parts and the coordinate in the y-direction of point n_i $(i = 1, 2, \ldots, t)$ is obtained by accumulating from the minimum point one by one. In order to ensure a continuous curvature at the symmetric line of the streamlined part, the free parameter n_v is set to 2, and for other curved surfaces, it is set to 1. As for calculation, first, the y-coordinate is calculated by formula (7), and then the z-coordinate is calculated by formula (8).

$$y(x) = y_{\min}(x) + \frac{n_i}{n_t}(y_{\max}(x) - y_{\min}(x)) \tag{7}$$

$$z(x, y) = z_{\min}(x) + \left(\frac{y}{y_{\max}}\right)^{n_y} z_{\max}(x) \tag{8}$$

where (y_{min}, z_{min}) and (y_{max}, z_{max}) are the coordinates of the control line of the curved surface.

The shape of the air guiding channel in the nose cone is not only the key factor affecting the aerodynamic performance of the high-speed maglev train but also the key factor to be considered in the aesthetics design. The air guiding channel is in a spatial 3D shape, which is controlled by formulas (9) and (10). The calculation method of coordinate points is the same as that of the spatial point interpolation.

$$y(x) = \frac{w_{10}}{2}\sin\left(\frac{x - x_{mmin}}{w_{12} - w_{11}}\pi\right) \times \left[\sin\left(\frac{y_n - y_{mmin}}{y_{mmax} - y_{mmin}}\pi\right)\right]^2 \tag{9}$$

$$z(x) = w_{10}\sin\left(\frac{x - x_{mmin}}{w_{12} - w_{11}}\pi\right) \times \left[\sin\left(\frac{z_n - z_{mmin}}{z_{mmax} - z_{mmin}}\pi\right)\right]^2 \tag{10}$$

where x_{mmin}, y_{mmin} and z_{mmin} are the minimum values in x, y and z directions, respectively; w_{10}, w_{11} and w_{12} are the design parameters of the air guiding channel in the nose cone.

A total of 12 critical design parameters are extracted through the parametric design of the high-speed maglev train shape: w_1 controls the length of the nose; w_2, w_3 and w_4 control the shape of L1; w_5, w_6 and w_7 control the shape of L2; w_8 and w_9 control the shape of L3; w_{10}, w_{11} and w_{12} control the shape of the air guiding channel near the nose cone. The range of each design parameter is shown in Table 1.

The high-speed maglev train nose corresponding to different design parameters is obtained with the parametric method, as shown in Figure 7. It can be seen from Figure 7 that different nose shapes can be obtained by adjusting the value of the design parameters; the basic profile of the nose depends on the lines that control the nose cone shape, and the profile of the nose can be adjusted by changing the air guiding mode of the nose cone. As a result, the nose of the high-speed maglev train can be described in detail by using the parametric design method, and this method can be used for the conceptual design and optimization design of the nose.

Design parameter	Range	Design parameter	Range
w_1	(10.0, 20.0)	w_7	(1.0, 3.0)
w_2	(0.2, 2.5)	w_8	(1.5, 2.0)
w_3	(0.5, 3.0)	w_9	(2.0, 3.0)
w_4	(0.5, 4.0)	w_{10}	(−25.0, 0.0)
w_5	(0.2, 2.5)	w_{11}	(20.0, 60.0)
w_6	(0.5, 3.0)	w_{12}	(80.0, 120.0)

Table 1. Critical design parameters and their range

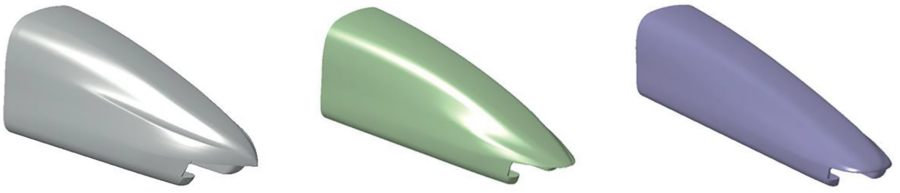

Scheme 1 **(a)** Scheme 2 **(b)** Scheme 3 **(c)**

Figure 7. Noses corresponding to different design parameters

3.3 Optimization results

The numerical calculation results are deemed as accurate results, and four test sample points are used to justify the prediction accuracy of the SVR model. The prediction errors of the four test sample points are shown in Table 2. In the table, CFD represents the numerical calculation results, and SVR represents the prediction results of the SVR model. According to Table 2, for each optimization objective, the prediction values of the SVR model are basically consistent with the trend of the numerical calculation results. The prediction error of the aerodynamic drag of the whole train is small. The average prediction error of the four test sample points is only 0.58%, the average prediction error and the maximum prediction error of the aerodynamic lift of the leading car are 7.96 and 12.42% respectively and the average prediction error and the maximum prediction error of the aerodynamic lift of the trailing car are 8.59 and 12.81% respectively. The prediction accuracy of each set of response surface model meets the design requirements.

The aerodynamic lift on the leading car and that on the trailing car of the high-speed maglev train are lifting force and have the same trend of changes. To be specific, when the aerodynamic lift on the leading car decreases, that on the trailing car also decreases, but the decrease amplitudes are different. In order to make the optimization algorithm easier, the aerodynamic drag coefficient of a three-car train and the aerodynamic lift coefficient of the trailing car are set as the optimization objectives. The aerodynamic lift coefficient of the leading car is used as the constraint condition for the multi-objective optimization. The constraint limit of the aerodynamic lift coefficient of the leading car is not more than 25% of the aerodynamic lift coefficient of the leading car in the original shape.

The multi-objective PSO is used for the optimization, and the Pareto solution set is obtained. The number of particle swarms is 200, the evolution generations are 5,000, the acceleration factor is 2, the inertia factor changes from 1.2 to 0.4 while the number of evolution generations increases and the maximum flying speed of particles is 0.1. The Pareto solution sets for the two objectives, i.e. the aerodynamic drag coefficient of the train and the aerodynamic lift coefficient of the trailing car are shown in Figure 8. According to Figure 8, in the design space, the optimal solution of the aerodynamic drag coefficient of the train spans in a narrow range and that of the aerodynamic lift coefficient of the trailing car spans in a wide range. This indicates that individuals in the Pareto solution set are different, and the diversity is higher. For the engineering design, there are more options available.

For the selection of the optimized shape, the sample point with balanced aerodynamic drag of the whole train and aerodynamic lift of the trailing car is preferred. Therefore, the design point P1 in Figure 8 is selected as the final optimized shape. The aerodynamic coefficients of the original and optimized shapes are shown in Table 3. According to Table 3, after optimization, the decrease in the aerodynamic lift coefficient of the leading car is 79.2%, and it is the maximum, and the decrease in the aerodynamic drag coefficient of the leading car is 27.4%, and it is the minimum; the decrease in the aerodynamic drag coefficient is similar to the decrease in the aerodynamic lift coefficient of the trailing car; both the aerodynamic drag

	Aerodynamic drag coefficient of train			Aerodynamic lift coefficient of leading car			Aerodynamic lift coefficient of trailing car		
Test sample	CFD	SVR	Error/%	CFD	SVR	Error/%	CFD	SVR	Error/%
Sample point 1	0.752	0.753	0.13	0.194	0.218	12.37	0.729	0.688	5.62
Sample point 2	0.723	0.723	0	0.203	0.214	5.42	0.685	0.612	10.66
Sample point 3	0.710	0.715	0.70	0.216	0.230	6.48	0.458	0.516	12.66
Sample point 4	0.713	0.719	0.84	0.178	0.195	9.55	0.610	0.626	2.62

Table 2.
Prediction error of SVR model

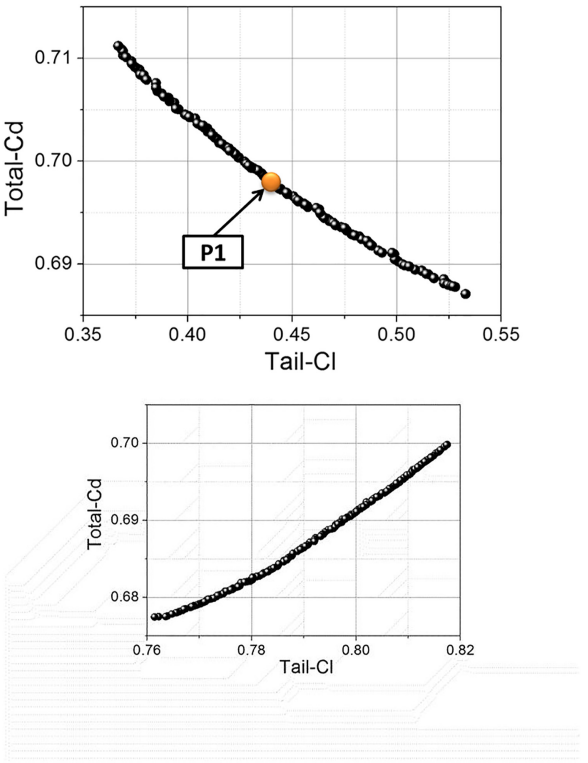

Figure 8.
Pareto solution sets for aerodynamic drag coefficient of train and aerodynamic lift coefficient of trailing car

Shape	Aerodynamic drag coefficient of train	Aerodynamic drag coefficient of leading car	Aerodynamic lift coefficient of leading car	Aerodynamic drag coefficient of trailing car	Aerodynamic lift coefficient of trailing car
Original shape	1.000	0.368	1. 000	0.439	0.734
Shape optimization	0.698	0.267	0.208	0.222	0.440
Decrease	31.2%	27.4%	79.2%	49.4%	40.1%

Table 3.
Aerodynamic coefficients in case of original and optimized shapes

coefficient and the aerodynamic lift coefficient of the high-speed maglev train greatly decrease, indicating that the optimization effect is good.

The surface pressure cloud diagrams of the original and optimized shapes of leading and trailing cars are shown in Figure 9. According to Figure 9, for the same nose, the leading car and the trailing car have basically the same surface pressure distribution. There is an obvious high-pressure zone at the nose tip and a low-pressure zone in the transition area between the streamlined part and the straight section of the carbody; compared with the original shape, the length of the nose in the optimized shape increases to 16 m, and the transition between the streamlined part and the straight section of the carbody is more smooth. The area and strength of the low-pressure zone here decrease significantly, resulting in a much lower aerodynamic lift on leading and trailing cars; after optimization, the nose tip changes from a

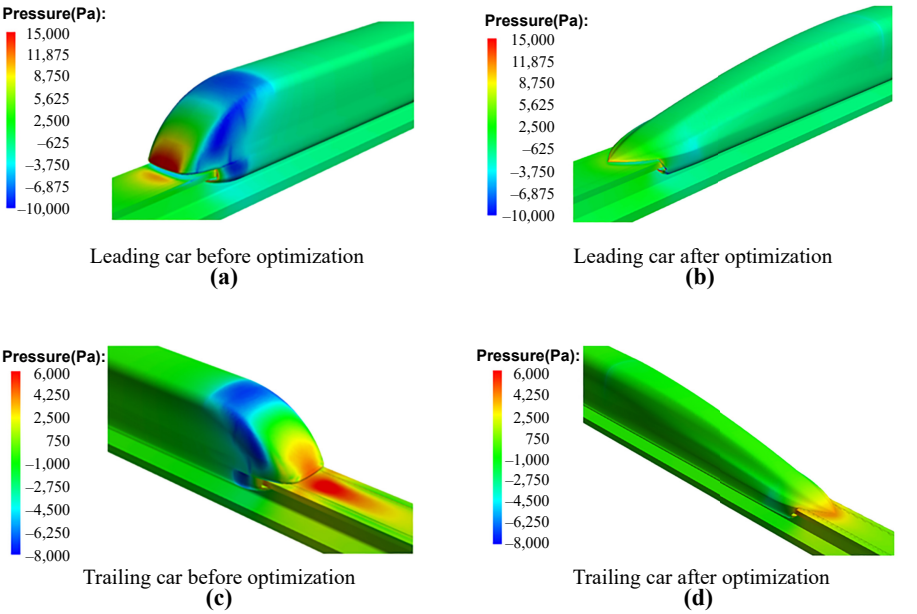

Figure 9.
Surface pressure cloud diagrams of original and optimized shapes

blunt tip to a sharp cone, and the area and strength of the high-pressure zone decrease significantly, resulting in a smaller pressure difference between leading and trailing cars.

In order to obtain the contribution of the design parameters to optimization objectives, the sensitivities of each design parameter to the aerodynamic drag coefficient of the train, the aerodynamic lift coefficient of the leading car and the aerodynamic lift coefficient of the trailing car are analyzed by using the finite difference method. The results are shown in Table 4. In the table, positive numbers indicate that the design parameters are positively correlated with optimization objectives; negative numbers indicate that the design parameters are negatively correlated with optimization objectives; the larger the absolute value of the numbers is, the greater the contribution of the design parameters will be.

It can be seen from Table 4 that w_3, w_6, w_8, w_{10} and w_{11} are positively correlated with the aerodynamic drag coefficient of the train, and other design parameters are negatively correlated with this coefficient; w_1 (controlling the nose length) makes the maximum contributions, followed by w_8 and w_9 (controlling the curve shape at the front end of equipment cabin); w_{10}, w_{11} and w_{12} (controlling the shape of the air guiding channel) make fewer contributions. w_3, w_6, w_8 and w_{10} are positively correlated with the aerodynamic lift coefficient of leading and trailing cars, and other design parameters are negatively correlated with this coefficient; w_8 controls the position of the upper endpoint of the curve at the front end of the equipment cabin and makes the maximum contributions; w_5, w_6 and w_7 control the horizontal section lines and make much higher contributions than w_2, w_3 and w_4, which control the longitudinal section lines; therefore, the shape design for the aerodynamic lift should focus on the influence of horizontal section lines.

In terms of the three optimization objectives, w_1 makes high contributions to the nose length, and it should be prioritized in the nose design; compared with longitudinal section lines, horizontal section lines have a greater influence on the aerodynamic performance of the train; the shape of the air guiding channel has a small influence on the aerodynamic performance of the train, so the depth of the air guiding channel should be mainly considered in the design.

Design parameter	Sensitivity to the aerodynamic drag coefficient of the train	Sensitivity to the aerodynamic lift coefficient of the leading car	10^{-4} Sensitivity to the aerodynamic drag coefficient of the trailing car
w_1	−18.7	−17.1	−17.3
w_2	−3.5	−15.2	−16.0
w_3	1.4	3.7	3.2
w_4	−1.3	−4.5	6.5
w_5	−2.5	−10.2	−11.0
w_6	3.7	15.5	20.0
w_7	−4.0	−16.0	−14.6
w_8	4.6	28.8	33.8
w_9	−4.2	−10.5	−8.6
w_{10}	2.1	5.6	5.8
w_{11}	1.1	−0.9	−0.7
w_{12}	1.2	−2.6	−1.4

Table 4.
Sensitivity of critical design parameters to aerodynamic coefficients

4. Engineering improvement design

4.1 Improvement method

Although the parametric design method of the nose described above can control the 3D shape of the high-speed maglev train nose, it is constrained by the manufacturing of the nose tip. To be specific, it cannot meet the requirement for the continuous curvature between various curved surfaces. At the same time, in order to improve the ergonomics in terms of aesthetics, it is necessary to carry out engineering improvement on the optimized shape. The improvement procedure is as follows:

(1) Thicken the nose tip according to the requirements of the manufacturing process of the leading car cab;

(2) Check the view angle of the cab. If it does not meet the ergonomics requirements, adjust the curvature of longitudinal section line L1 of the nose as appropriate;

(3) Check whether the connection between the upper curved surface of the nose and the curved surface of the equipment cabin meets the requirement of continuous curvature. If not, adjust the connection between the curved surfaces until the curvature of the two curved surfaces is continuous;

(4) Check the shape of the air guiding channel at the nose tip. If the characteristics of the shape of the air guiding channel do not match the nose aesthetics, modify the shape as appropriate.

The 3D nose and the exterior design rendering after the engineering improvement of the optimized shape are shown in Figure 10. It can be seen from Figure 10 that the improved nose has a much better aesthetic effect and is feasible in terms of engineering.

4.2 Verification by wind tunnel test

In order to further verify the aerodynamic performance after the high-speed maglev train nose is optimized, a test was carried out on the 1:8 scale-down models of the original shape and the optimized shape after engineering improvement of a three-car train in the 8×6 m wind tunnel of Aerodynaiviics Research Institute (AVIC) Aerodynamics Research Institute. Refer to Figure 11 for the wind tunnel test site.

Without affecting the comparison, the wind tunnel test data of the original shape and that of the optimized shape after engineering improvement are divided by the wind tunnel test

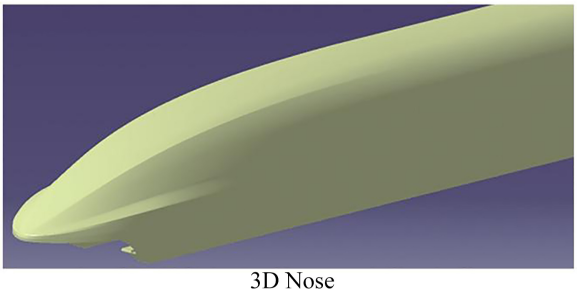

3D Nose

(a)

Exterior Design Rendering

(b)

Figure 10.
Nose after engineering improvement

Figure 11.
Wind tunnel test site

data of the original shape, and the results are shown in Table 5. From Table 5, it can be seen that compared with the original shape, the aerodynamic drag coefficient of the train after the engineering improvement of the optimized shape decreases by 19.2%, the aerodynamic lift coefficient of the leading car decreases by 24.8% and the aerodynamic lift coefficient of the trailing car decreases by 51.3%.

The decrease range of the aerodynamic coefficients in the wind tunnel test is greatly different from that in Table 2. There are two main reasons: (1) the optimized shape after

Table 5.
Aerodynamic drag and lift coefficients in wind tunnel test

Nose	Aerodynamic drag coefficient of train	Aerodynamic lift coefficient of leading car	Aerodynamic lift coefficient of trailing car
Original shape	1.000	1.000	1.000
Shape optimization	0.808	0.752	0.487
Decrease	19.2%	24.8%	51.3%

engineering improvement has a blunt nose tip, resulting in higher aerodynamic drag; (2) the wind tunnel test cannot simulate the influence of the ground effect on the aerodynamic performance of the train, while the ground effect has a great influence on the aerodynamic lift, resulting in a larger decrease amplitude in the aerodynamic lift coefficient of leading and trailing cars. The aerodynamic performance improvements of the optimized shape before and after the engineering improvement are different. However, the aerodynamic performance is greatly improved for both the optimized shapes compared with the original shape, indicating that the optimization method proposed above is applicable to the engineering design of the high-speed maglev train nose.

5. Conclusion

(1) By changing the high-speed maglev train nose, the aerodynamic performance of the train can be effectively improved. The study is carried out based on a three-car high-speed maglev train. A total of 12 critical design parameters are extracted with the improved VMF parametric method. Based on the response surface model of the SVR and the multi-objective PSO, the aerodynamic drag coefficient of the train and the aerodynamic lift coefficient of the trailing car are set as the optimization objectives, and the aerodynamic lift coefficient of the trailing car is used as the constraint condition to carry out the nose optimization design of the high-speed maglev train. The nose optimization design process of high-speed maglev trains is proposed, and the Pareto solution sets for various optimization objectives are obtained. The solution with balanced aerodynamic drag of the train and aerodynamic lift of the trailing car is selected as the optimized shape, and the sensitivity analysis method is used to determine the contributions of each design parameter to the optimization objectives.

(2) The parametric method can describe the high-speed maglev train nose in detail; the response surface model of the SVR can effectively reduce the flow field calculations and significantly improve the optimization efficiency; the nose length makes high contributions to each optimization objective, and so it should be prioritized in the nose design. Compared with the longitudinal section lines, the horizontal section lines have a greater influence on the aerodynamic performance of the high-speed maglev train.

(3) Compared with the original shape, the aerodynamic drag coefficient of the train decreases by 19.2%, the aerodynamic lift coefficient of the leading car decreases by 24.8% and that of the trailing car decreases by 51.3% after the optimized shape is improved according to the engineering design requirements.

References

Bi, H., Lei, B., & Zhang, W. (2004). Research on numerical calculation for aerodynamic characteristics of the TR maglev train. *Journal of the China Railway Society*, *26*(4), 51–54, in Chinese.

Britcher, C. P., Wells, J. M., & Renaud, B. (2012). Aerodynamics of urban maglev vehicles. *Proceedings of the Institution of Mechanical Engineers, Part F: Journal of Rail and Rapid Transit*, *226*(6), 561–567.

Ding, S., Yao, S., & Chen, D. (2020). Aerodynamic lift force of high-speed maglev train. *Journal of Mechanical Engineering*, *56*(8), 228–234, in Chinese.

Gong, M., Sun, S., & Li, Q. (2019). Multi-objective optimization design for nose shape of high speed train in cross wind conditions. *China Railway Science*, *40*(2), 97–106, in Chinese.

Ku, Y.C., Park, H.I., Kwak, M.H. (2010). Multi-objective optimization of high-speed train nose shape using the vehicle modeling function. *48th AIAA Aerospace Sciences Meeting Including the New Horizons Forum and Aerospace Exposition*, Orlando: AIAA.

Li, R., Liu, Y., & Zhai, W. (2004). Numerical analysis of aerodynamic force in longitudinal and vertical direction for high-speed maglev train. *China Railway Science*, *25*(1), 8–12, in Chinese.

Liu, T., Tian, H., & Wang, C. (2006). Aerodynamic performance comparison of several kind of nose shapes of maglev train. *Journal of National University of Defense Technology*, *28*(3), 94–98, in Chinese.

Ma, J., Zhou, D., & Zhao, L. (2013). The approach to calculate the aerodynamic drag of maglev train in the evacuated tube. *Journal of Modern Transportation*, *21*(3), 200–208.

Rho, J.H., Ku, Y.C., & Kee, J.D. (2009). Development of a vehicle modeling function for three-dimensional shape optimization. *Journal of Mechanical Design*, *131*(12), 121004.

Shao, Y., Zhang, C., & Yang, Z. (2013). An ε -twin support vector machine for regression. *Neural Computing and Applications*, *23*(1), 175–185.

Shu, X., Gu, C., Liang, X. (2006). Numerical simulation and parameterized investigation of aerodynamic drag performances of high-speed maglev trains. *Journal of Traffic and Transportation Engineering*, *6*(2), 6–10, in Chinese.

Tielkes, T. (2006). Aerodynamic aspects of maglev systems. *19th International Conference on Magnetically Levitated Systems and Linear Drives*, Dresden, Germany.

Yao, S., Guo, D., & Yang, G. (2012). Three-dimensional aerodynamic optimization design of high-speed train nose based on GA-GRNN. *Science China Technological Sciences*, *55*(11), 3118–3130.

Yao, S., Guo, D., Sun, Z., Chen, D., & Yang, G. (2016). Parametric design and optimization of high speed train nose. *Optimization and Engineering*, *17*(3), 605–630.

Yao, S., Guo, D., Sun, Z., Yang, G., & Chen, D. (2014). Optimization design for aerodynamic elements of high speed trains. *Computers and Fluids*, *95*, 56–73.

Yang, G., Guo, D. L., Yao, S.B., & Liu, C.H. (2012). Aerodynamic design for China new high-speed trains. *Science China: Technological Sciences*, *55*(7), 1923–1928.

Yau, J.D. (2010). Aerodynamic vibrations of a maglev vehicle running on flexible guideways under oncoming wind actions. *Journal of Sound and Vibration*, *329*(10), 1743–1759.

Corresponding author
Shuanbao Yao can be contacted at: ysbao566@163.com